1-1-2019

Theory and simulation of spectral line broadening by exoplanetary atmospheric haze

Z. Felfli
Institute for Theoretical Atomic, Molecular and Optical Physics

T. Karman
Institute for Theoretical Atomic, Molecular and Optical Physics

V. Kharchenko
Institute for Theoretical Atomic, Molecular and Optical Physics

Daniel Vrinceanu
daniel.vrinceanu@tsu.edu

J. F. Babb
Institute for Theoretical Atomic, Molecular and Optical Physics

See next page for additional authors

Monthly Notices
of the
ROYAL ASTRONOMICAL SOCIETY

MNRAS **482,** 1330–1337 (2019)
Advance Access publication 2018 October 4

doi:10.1093/mnras/sty2694

Theory and simulation of spectral line broadening by exoplanetary atmospheric haze

Z. Felfli,[1,2] T. Karman,[1,3] V. Kharchenko,[1,4] D. Vrinceanu,[5] J. F. Babb[1] and H. R. Sadeghpour[1]★

[1]*ITAMP, Harvard – Smithsonian Center for Astrophysics, Cambridge, MA 02138, USA*
[2]*Department of Physics, Clark Atlanta University, Atlanta, GA 30314, USA*
[3]*Joint Quantum Centre, Durham University, Durham DH1 3LE, UK*
[4]*Department of Physics, UConn, Storrs, CT 06269, USA*
[5]*Department of Physics, Texas Southern University, Houston, TX 77004, USA*

Accepted 2018 October 2. Received 2018 August 28; in original form 2018 May 23

ABSTRACT

Atmospheric haze is a leading candidate for opacity and lack of prominent features in expolanetary spectra, as well as in the atmospheres of Solar system planets, satellites, and comets. Exoplanetary transmission spectra, which carry information about how the planetary atmospheres become opaque to stellar light in transit, often show broad absorption in the region of wavelengths corresponding to spectral lines of sodium, potassium, and water. We develop a detailed atomistic model, describing interactions of atomic or molecular radiators with dust and atmospheric haze particulates. This model incorporates a realistic structure of haze particulates from small nano-sized seed particles up to submicron irregularly shaped aggregates and accounting for both pairwise collisions between the radiator and haze perturbers, and quasi-static mean-field shift of atomic levels in haze environments. This formalism can explain large flattening of absorption and emission spectra in hazy atmospheres and shows how the radiator – haze particle interaction affects the absorption spectral shape in the wings of spectral lines and near their centres. The theory can, in principle, account for nearly all realistic structure, density, size, and chemical composition of haze particulates. We illustrate the utility of the method by computing shift and broadening of the emission spectra of the Na I D lines in haze environment, formed by Ar nano-clusters. Argon is used as the illustrative haze constituent only because of the simplicity of closed-shell atoms and their clusters for quantum mechanical calculations of interaction between radiator and nano-sized haze particles. The elegance and generality of the proposed model should make it amenable to a broad community of users in astrophysics and chemistry.

Key words: line: profiles – planets and satellites: atmospheres.

1 INTRODUCTION

Extrasolar planets (exoplanets) are being discovered at a breakneck pace, supplanting and transforming our understanding of planetary formation and habitability. Thousands of exoplanets have been identified using a host of detection techniques, through measurements of radial velocities, transits, and lensing (Encyclopaedia 2018; Wright et al. 2011, Also see http://exoplanets.org/). Many of these observed planets harbour atmospheres, and will be amenable to further observations with the launch of next generation telescopes, including the James Webb Space Telescope, the Transiting Exoplanet Survey Satellite, and with future terrestrial telescopes, including the Giant Magellan Telescope. An Analysis of spectral compositions and parameters of exoplanetary atmospheres is a topic of high interest, but prominent spectral features in observed transmission spectra of such exoplanets are often obscured.

Atmospheric haze is a leading candidate for the flattening of spectral transmission of exoplanetary occultation, a fact that is supported by observations of Solar system planets, including Earth, and cometary atmospheres (Seager & Deming 2010; Deming & Seager 2017; Zhang, Strobel & Imanaka 2017). Spectra transmitted through hazy atmospheres carry information about how these atmospheres become opaque to stellar light in transit (Pont et al. 2008; Deming & Seager 2017; Spake et al. 2018). Recent laboratory experiments simulating hazy environments for super-Earths and mini-Neptunes

★ E-mail: hsadeghpour@cfa.harvard.edu

atmospheres suggest that some of these atmospheres contain thick photochemically generated hazes (Hörst et al. 2018). Because hazy environments can reflect and absorb light, their conditions ought to be explored for direct imaging of exoplanets (Morley et al. 2015).

The stellar flux occultation during a planet's transit can also give clues to the persistence of an atmosphere; the wavelength-dependent measurement of the planet transit depths reveal information on atmospheric atomic and molecular composition and transparency of the atmosphere. The Na I D and K I first resonance lines were modelled in absorption to constrain line-of-sight atmosphere barometric parameters and cloud depths (Seager & Sasselov 2000). Predictions made by Seager & Sasselov (2000) were based on the assumption that these exoplanetary atmospheres are similar to brown and cool L dwarfs with similar effective temperatures. Water is expected to be the most spectroscopically active gas, but Na I, K I, metastable He I, and CO have been identified in hot Jupiter atmospheres, and in particular in HD 209458b, HD 189733b, and WASP-103b (Pont et al. 2008, 2013; Seager & Deming 2010; Sing et al. 2011; Deming & Seager 2017; Lendl et al. 2017; Spake et al. 2018). Many of the detected lines are model-dependent, but Na I (and K I) resonant doublets are not, as there are no other absorbers at such wavelengths.

In methane dwarfs (Burrows, Marley & Sharp 2000; Burrows et al. 2001), the K I doublet $4^2S - 4^2P$ absorption line at 769 nm is broad and is responsible for large continuum depression, red shifted in optical spectra. The continuum broadening is induced due to collisional interaction (pressure broadening) between the radiator and background gas atoms and molecules. This lower than expected contrast of the strength of the alkali metal lines (Fortney et al. 2003) has been puzzling: subsolar elemental abundances, stellar radiation ionization, and atmospheric haze particulates have been invoked as sources for the diminished strength of the lines.

The haze hypothesis has gained currency (Burrows 2014; Deming & Seager 2017). Spectra observed from different planetary and exoplanetary atmospheres, comets, and natural satellites reveal unusual lack of sharp spectral features, attributed to the presence of atmospheric dust, ice, and haze particles (Tomasko, Karkoschka & Martinek 1986; West 1991; Ortiz, Moreno & Molina 1996; Greenberg & Li 1999; Rannou, Hourdin & McKay 2002; Wong, Yung & Friedson 2003). A compelling evidence for the direct role played by haze layers in flattening of the exoplanetary lines is the transit spectra of HD189733b in near-UV and mid-IR by Pont et al. (2013, 2008). Lack of features in the range from 550 to 1050 nm in the spectra of HD 189733b is suggestive of extinction by condensates high in the atmosphere (Pont et al. 2008). In general, hazes are mostly small (submicron) cluster particulates that can produce a broad continuum opacity to light. Interaction between haze particles and radiating atoms or molecules can dramatically modify absorption spectra of exoplanets. The red hue of Jupiter is likely produced by unidentified trace species or haze (Burrows 2014). The transit spectra for the mini-Neptune GJ 1214b have been shown by Kreidberg et al. (2014) to be 5–10 times flatter than in a water-rich, H_2-dominated atmosphere, heralding the presence of a thick layer of haze, or other high molecular weight gas. *In situ* measurements of the effective density of aerosol materials in analogue Titan atmospheres confirm values of $\sim$0.4–1.13 g cm^{-3}, which for a methane-dominated hazy environment, translates to atomic/molecular densities of a few times 10^{22} cm^{-3} (Hörst & Tolbert 2013).

We present a theoretical framework for a quantum mechanical description of the shift and broadening of atomic and molecular spectral lines by dust and haze particles at densities relevant to hazy planetary atmospheres. Our model can be applied to shift and broadening analysis of different lines of atomic and molecular spectra, when haze particulates have liquid or solid structures or consist of high porosity materials (Vinatier et al. 2018). Spectral calculations are obtained through the introduction of the pseudo-potential for the interaction between radiator electrons and atoms and molecules of haze particles (Szasz 1985). The pseudo-potential method allows us to carry out calculations for different chemical compositions of haze (Boatz & Mario 1994; Jacquet et al. 2011). The binary collision between the radiator and haze particulate, affecting the radiator line centre, is also considered (Allard & Kielkopf 1982).

2 METHODOLOGY

2.1 Modelling of emission and absorption spectra in haze environments

The physical nature, composition, and structure of these particles is roughly known for the Earth, some Solar system planets, satellites, and comets (West 1991; Greenberg & Li 1999; Seignovert et al. 2017), but for exoplanetary atmospheres the nature of the particles is not known (Tinetti et al. 2007). Analysis and interpretation of atomic and molecular spectra observed from dusty environments is a formidable task because of complicated quantum mechanical interaction between radiating atoms/molecules and haze particles.

Another fundamental obstacle in modelling optical properties of mesoscopic dust, ice, and haze particles is the stochastic nature of the haze particle distribution (Greenberg & Li 1999; Sciamma-O'Brien, Upton & Salama 2017). A review on cloud modelling, and scattering and extinction efficiencies of cloud particles in terrestrial climates, gas giants, and brown dwarfs is given in Marley et al. (2013). The simplest approaches to modelling distributions employ empirically assigned refractive indices in the classical Mie model for scattering and absorption of radiation by spherical haze particles (Lenoble, Mishchenko & Herman 2013; Seignovert et al. 2017). This model fails to describe realistic changes in atomic and molecular emission/absorption spectra because optical properties of nano-sized particles cannot be described by macroscopic parameters such as the refractive index.

2.2 Quantum mechanical model of interaction between radiator and haze particles

The electronic Hamiltonian $H_{\rm el}$ for the radiator-haze system can be written as

$$H_{\rm el} = H_r + H_{\rm hp} + V_{\rm r-hp}, \quad (1)$$

where H_r is an electronic Hamiltonian of radiating atom or molecule; $H_{\rm hp}$ the haze particle Hamiltonian, and $V_{\rm r-hp}$ the potential of interaction between the haze and radiator electrons. The haze particle Hamiltonian $H_{\rm hp}$ includes kinetic energies and interaction potential energies of all atomic and molecular constituents.

The term $V_{\rm r-hp}$ is given by the sum of interaction potential energies $V_{\rm i}$ between radiator electrons and an atomic or molecular constituent in the haze at location $\boldsymbol{R}_{\rm i}$: $V_{\rm r-hp} = \sum_{i=1}^{N} V_{\rm i}(\boldsymbol{r}_{\rm e}, \boldsymbol{R}_r, \boldsymbol{R}_{\rm i})$, where N is the total number of haze atoms and/or molecules, $\boldsymbol{r}_{\rm e}$ is the electron coordinate from the radiator centre $\boldsymbol{R}_r$. Fig. 1 illustrates the basic configuration of the haze-radiator system.

There are only dozens of atoms or molecules in nano-sized seed particles and millions in submicron haze aggregates. The set of location vectors $\{\boldsymbol{R}_{\rm i}\}$ determines the geometrical structure of haze, its physical properties, and characteristics of interaction with radiator. For a mesoscopic-sized 'haze-radiator' system, the

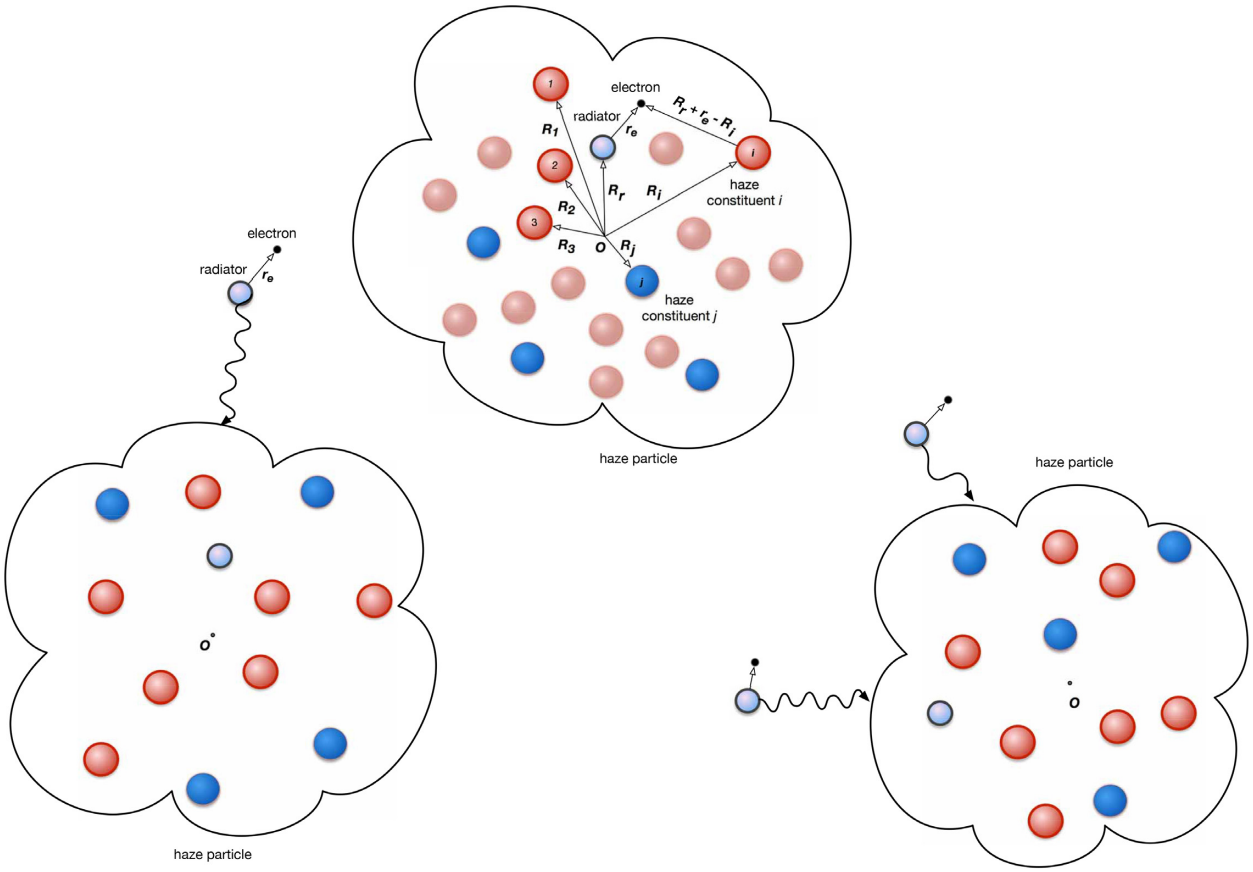

Figure 1. A diagram of haze particles of arbitrary shape interacting with radiator atoms. The active radiator electron, $\boldsymbol{r}_e$, interacts with the radiator core, $\boldsymbol{R}_r$, and with all other atoms within the haze at positions $\boldsymbol{R}_i$. Haze constituents of different chemical compositions are denoted with red and blue spheres. The density of haze atomic/molecular constituents is denoted by $\rho(R_{i,j})$, and Gaussian distributed in this work. Photons are indicated with wiggly arrows.

set $\{\boldsymbol{R}_i\}$ has typically an irregular structure and resembles an amorphous or liquid cluster. Nevertheless, seed particles could be represented by nanocrystals or amorphous Si or C materials covered by polycrystalline structures of H_2O and CO_2 ices or CH_4 droplets expected as outer shells in highly porous submicron haze aggregates.

2.2.1 *Mean-field spectral line shift in haze environment*

The atmospheric distribution of haze particles is non-uniform as is the distribution of atoms and molecules inside haze droplets. Our modelling of spectral line shift and broadening is focused on the quantum mechanical description of the interactions between the haze particles and the atomic or molecular radiators. The many-body interaction between the emitter and haze constituents is considered in the mean-field approximation.

The Fermi pseudo-potential method (Fermi 1934) was first developed to describe the species-dependent mean-field pressure shift and broadening of Rydberg lines in gaseous environments and more recently in the context of Rydberg molecule formation in ultracold quantum gases (Greene, Dickinson & Sadeghpour 2000, Shaffer, Rittenhouse & Sadeghpour 2018).

The Fermi pseudo-potential is defined proportional to the scattering length L_i of the radiator electron from the ith haze perturber (Fermi 1934), see Fig. 1,

$$V_i(\boldsymbol{r}_e, \boldsymbol{R}_r, \boldsymbol{R}_i) = \frac{2\pi\hbar^2}{m_e} L_i \delta(\boldsymbol{R}_r + \boldsymbol{r}_e - \boldsymbol{R}_i), \quad (2)$$

where $\boldsymbol{r}_e$ is the radiator electron coordinate, L_i is the scattering length of the electron of mass m_e colliding with the haze atom/molecule at $\boldsymbol{R}_i$, $\hbar$ is the reduced Planck constant, and $\delta()$ is the Dirac delta-function. The chemical composition of haze particles is represented by a set of individual scattering lengths $\{L_i\}$. The scattering length is obtained from the zero-energy limit of the scattering phase shift. Presence of perturbers in the vicinity of radiator modifies the radiator wavefunction and energy spectra that finally leads to changes in energy and rates of emitted/absorbed photons.

Models of spectral shift and broadening (Allard & Kielkopf 1982; Szudy & Baylis 1996) describe the influence of collisional or quasi-static interaction potentials on emission and absorption spectra. In the quasi-static approach, the line shift $\Delta\omega = \omega - \omega_0$ induced in binary interaction is equal to the difference of radiator electron energies as a function of the perturber-radiator distance, i.e. $\hbar\Delta\omega = \Delta V(R)$, where $\Delta V(R)$ is the difference of the ground and excited Born – Oppenheimer potential energies, e.g. Section 2, induced by the perturber. The inverted equation $R_C = R(\Delta\omega)$ yields the location of Condon points, resulting in specific frequency shifts $\Delta\omega$. For the simplest case of cold and dilute gas of uniformly distributed perturbers, the intensity of the spectral line is proportional to the probability to find a perturber at distances between R and $R + \mathrm{d}R$, i.e. $I(\Delta\omega) = 4\pi\rho R^2(\Delta\omega)|\frac{\mathrm{d}R(\Delta\omega)}{\mathrm{d}(\Delta\omega)}|$, with ρ the perturber density (Allard & Kielkopf 1982). Haze particles and aggregates may be considered as an environment of slow perturbers with a large and essentially non-uniform perturber density $\rho(R)$.

The mean-field model in this work is also applicable to calculations of collisional shift and broadening inside haze aggregate particles with high levels of porosity (∼90 per cent). Collisional and mean-field mechanisms dominate in different regions of emission and absorption spectra. Interaction between haze particles and radiator can provide significant shifts of atomic and molecular lines in extreme cases up to 10^4 cm^{-1} (Jacquet et al. 2011) depending on the radiator position.

Analytical formulas for the shifted electron energies $\epsilon_{\rm i,f}(\boldsymbol{R}_r)$ of a radiator in the ground (initial) and excited (final) states obtained from the leading term of the perturbation theory:

$$\epsilon_{i,\rm f}(\boldsymbol{R}_r) = \epsilon^0_{i,\rm f} + \langle\Psi_{i,\rm f}(\boldsymbol{r}_{\rm e})|V_{i,\rm f}|\Psi_{i,\rm f}(\boldsymbol{r}_{\rm e})\rangle = \epsilon^0_{i,\rm f} + \frac{2\pi\hbar^2}{m_{\rm e}}\sum_{i=1}^{N} L_{\rm i}|\Psi_{i,\rm f}(\boldsymbol{r}_{\rm e}=\boldsymbol{R}_{\rm i}-\boldsymbol{R}_r)|^2, \quad (3)$$

where $\Psi_{\rm i}$ and $\Psi_{\rm f}$ are wavefunctions of the ground and excited states of free (unperturbed) radiator atoms and $\epsilon^0_{i,\rm f}$ are related electronic energies. For systems with high densities of perturbers, such as haze ice, dust or liquid droplets, the perturbation can be strong and radiator electronic wavefunctions need be renormalized according to the mean field induced by the perturbers (Demkov & Ostrovskii 1988). For haze particles and aggregates with a large number of equivalent atoms or molecules N, the summation in equation (3) can be replaced with integration over the volume of the haze aggregate with a specific volume density $\rho(\boldsymbol{R})$. For a collection of N identical perturbers, the Born – Oppenheimer electronic energies of the radiator $\epsilon_{\rm i,\,f}$ for initial i- and final f states are calculated as

$$\epsilon_{\rm i,f}(\boldsymbol{R}_r) = \epsilon^0_{\rm i,f} + V_{\rm i,f}(\boldsymbol{R}_r) = \epsilon^0_{\rm i,f} + \frac{2\pi\hbar^2}{m_{\rm e}} L_{\rm i} N \times \int {\rm d}\boldsymbol{r}_{\rm e}\,\rho(\boldsymbol{r}_{\rm e}+\boldsymbol{R}_r)\,|\Psi_{\rm i,f}(\boldsymbol{r}_{\rm e})|^2, \quad (4)$$

where $\rho(\boldsymbol{R}_p)$ is the unit normalized spatial distribution function in the haze droplet at $\boldsymbol{R}_p = \boldsymbol{r}_{\rm e} + \boldsymbol{R}_r$. The mean-field potential $V_{\rm i,f}(\boldsymbol{R}_r)$ induced by the haze particles depends on the symmetry of electronic states and symmetry of the perturber distribution function $\rho(\boldsymbol{R}_p)$. This potential can be a function of the radiator coordinate $\boldsymbol{R}_r$. The spectral intensity $I(\Delta\omega)$ is expressed via mean-field energy shifts:

$$I(\Delta\omega) = \int d^3R_r\; p(\boldsymbol{R}_r)\,\delta(\Delta\omega - [V_{\rm f}(\boldsymbol{R}_r) - V_{\rm i}(\boldsymbol{R}_r)]/\hbar), \quad (5)$$

where $p(\boldsymbol{R}_r)$ is the unit normalized distribution function of radiators inside and outside haze droplet. The replacement of $p(\boldsymbol{R}_r)$ with the radiator partition function can provide a temperature dependence of the radiator spatial distribution. Angular anisotropy of the mean-field potentials $V_{\rm i,f}(\boldsymbol{R}_r)$ plays an important role in integration of the δ-function in equation (5). For spherically symmetric Born – Oppenheimer energy splitting $\Delta V(R_r) = V_{\rm f}(\boldsymbol{R}_r) - V_{\rm i}(\boldsymbol{R}_r)$, the expression for $I(\Delta\omega)$ formally reduces to the known approximation (Allard & Kielkopf 1982).

2.2.2 *Shift and broadening of spectral line in binary collisions*

The mean-field spectral shift represents only a part of the total shift and broadening of unperturbed spectral line with frequency $\omega_0 = \Delta\epsilon_0 = \epsilon^0_{\rm i} - \epsilon^0_{\rm f}$. Collisional effects are thermally driven, and hence temperature-dependent. In the relatively dense environments, the binary collision between the radiator and a nearby perturber happens in the presence of mean-field shifts induced by large number of other slowly moving perturbers. The temperature-dependent binary collision broadening and shift rates are, respectively, $\rho(\boldsymbol{R}_r)\gamma(T)$ and $\rho(\boldsymbol{R}_r)\sigma(T)$ (Allard & Kielkopf 1982; Vrinceanu, Kotochigova & Sadeghpour 2004).

The overall line shape is obtained upon integrating the localized contributions over the whole volume, assuming that the radiator is found at position $\boldsymbol{R}_r$ with the spherically symmetric probability density $p(\boldsymbol{R}_r)$:

$$I(\omega) = \frac{1}{\pi}\int_0^\infty \frac{\rho(\boldsymbol{R}_r)\gamma}{[\omega - (\Delta\epsilon_0 + V_{\rm f}(\boldsymbol{R}_r) - V_{\rm i}(\boldsymbol{R}_r)) - \rho(\boldsymbol{R}_r)\sigma]^2 + [\rho(\boldsymbol{R}_r)\gamma]^2} \times\; p(\boldsymbol{R}_r)\,d^3R_r. \quad (6)$$

In the above, the first term in the denominator describes the shift of the resonance frequency ω_0, and the second term the broadening.

We expect a strong transformation of the emission spectra when the radiator is localized near the surface or inside haze aggregate. In such cases, the strong mean-field interaction creates a broad emission/absorption spectra, significantly shifted from the unperturbed line at ω_0. The spectral regions with the photon frequencies near the unperturbed spectral lines are mostly formed by collisional interactions with shifted and broadened Lorentzian profiles (Szudy & Baylis 1996; Vrinceanu et al. 2004), and become temperature-dependent.

The rich experimental and theoretical database on collisional transformation of emission and absorption spectra are available for different atomic and molecular radiators in a gas environment (Szasz 1985; Vrinceanu et al. 2004), where physics of shift and broadening of spectra near the radiator spectral core is described by binary collisions between radiators and gas particles. Analysis of spectral line shift and broadening provides valuable information on parameters of atmospheric gases and haze particles. Parameters of the collisional and mean-field mechanisms of the shift and broadening for different spectral lines can yield unique vistas on physical characteristics of haze particle size, shape, and material.

3 ILLUSTRATIVE RESULTS

Compositions and parameters of haze particle and atmospheric gases are expected to vary considerably for different exoplanets. Nevertheless, the influence of haze nano-particles on spectra has certain common features despite specific properties of exoplanetary and planetary atmospheres. These common characteristics reflect the quantum-mechanical nature of interaction between radiator and nano-sized objects and, with for illustrative purposes, can be investigated for the simplest haze environment: cool noble gas with embedded atomic nano-sized atomic droplets and clusters, such as $\rm He_N$, $\rm Ne_N$, $\rm Ar_N$, and $\rm Xe_N$. We demonstrate the utility of the current theoretical framework for hazy expolanetary atmospheres, using a sodium atom as the resonant radiator and argon as the haze constituent at realistic measured haze particle densities. We emphasize that while no haze constituents in Titan or exoplanetary atmospheres are made of Ar, the simplicity afforded by using closed-shell atoms, such as argon, of complex quantum mechanical Born – Oppenheimer potential energy curves, e.g. Fig. 2, serves to quantitatively illustrate the different shift mechanisms at play. Furthermore, argon nanoclusters are more readily accessible in the lab.

The electron scattering length for argon has been measured from low-energy drift velocities of electrons in an H-Ar mixture, to be $L_{\rm Ar} = -1.46\ a_0$, (Petrovic, O'Malley & Crompton 1995), where a_0 is the Bohr radius. Admittedly, the haze constituency will more likely be in the form of carbon-bearing, water, and other complex molecules, but for purposes of computational efficiency, interacting sodium atoms with rare-gas atomic samples offers a convenient way

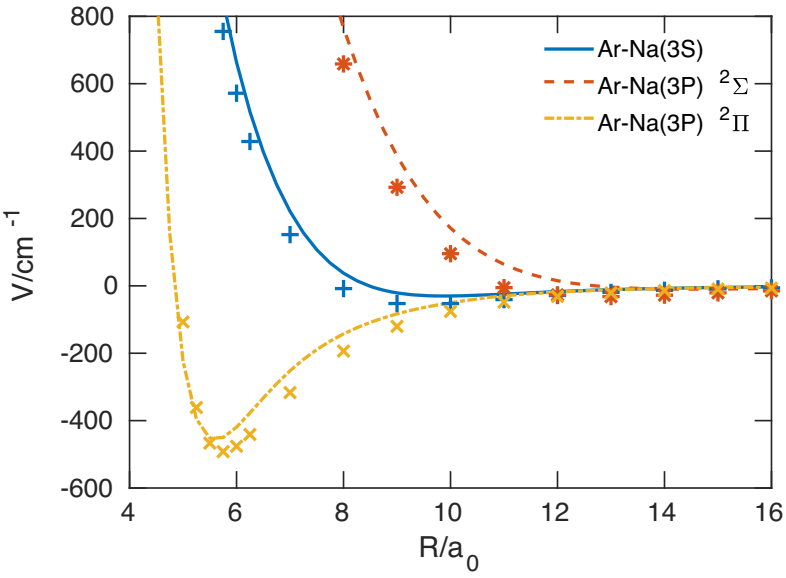

Figure 2. Potential energy curves for Ar−Na(3S,3P). The Na I D line energy is subtracted. Lines correspond to the potential energy curves calculated in this work, and symbols correspond to calculated potential energy values (Saxon, Olson & Liu 1977).

to calculate the many-body mean-field aspect of this theory. Below, we describe how we calculate the binary interaction in Na-Ar.

3.1 Binary potential energy curves

We employ effective core potentials (ECPs), developed by Nicklass et al. (1995), to represent the 10 core electrons for argon and sodium atoms. The sodium core dipole polarizability is $\alpha = 0.9947$ and exponential cutoff parameter $\delta = 0.62$, in atomic units, using the core polarization potentials (CPPs) developed by Fuentealba et al. (1982) and implemented in MOLPRO (Werner et al. 2012). The one-electron basis set for the valence electrons of the argon perturber is taken from Nicklass et al. (1995). The sodium radiator is described using an extended one-electron basis set, defined as follows: the s, p, and d orbitals are represented by a set of uncontracted 5 Gaussians with even-tempered exponents between 1.0 and 0.01 atomic units. Two sets of uncontracted Gaussian f orbitals with exponents 0.08. and 0.008 are also included.

We perform complete active space self-consistent field (CASSCF) calculations to obtain molecular orbitals, state-averaged over the 3S ground state, and 3P excited states. The active space contains the nine valence electrons in argon and sodium $3s$ and $3p$ orbitals. Subsequently, we perform multireference configuration interaction (MRCI) calculations, which include single and double excitations from this active space. The Pople size-consistency correction is added, and the interaction energies are calculated using the counterpoise procedure of Boys & Bernardi (1970), to correct for the basis set superposition error. We use a dense grid in the radial coordinate, extending from $R = 3$ to 20 a_0 in steps of 0.25 a_0, with additional points at 22, 25 a_0. A final point at $R = 50$ a_0 is used to subtract any remaining error in size consistency. All calculations are performed using the MOLPRO suite of *ab initio* programs (Werner et al. 2012).

The potential energy curves are shown in Fig. 2. Results obtained in this work are shown as lines. There are two potentials correlating to the Na(3P) excited state. The $^2\Sigma$ ($^2\Pi$) potential governs the interaction if the excited valence electron occupies a 3P orbital oriented parallel (perpendicular) to the interatomic axis. The $^2\Pi$ excited state potential is significantly more attractive, with a well depth of around 450 cm^{-1}, and becomes repulsive only for much shorter interatomic separations. The $^2\Sigma$ excited state, however, has a more repulsive potential than the ground state. The calculated potentials are in good qualitative agreement with the results of Saxon et al. (1977).

3.2 Shift and broadening of Na line in Ar haze

The argon droplet is modelled by a Gaussian distribution, given by a spherically symmetric position-dependent density $\rho(R) = [N_{\rm Ar}/(2\pi a^2)^{3/2}]\exp(-R^2/2a^2)$, which depends on the droplet size parameter a, and the number of Ar atoms, $N_{\rm Ar}$. A sodium atom at a distance R_r from the centre of the droplet has a shifted Lorentz absorption profile as in equation (6), where the shape of the line is determined by two contributions: (a) mean-field quasi-static contribution of neighbouring argon atoms that produce the energy shifts $\Delta V(R_r) = V_{3P}(\boldsymbol{R}_r) - V_{3S}(\boldsymbol{R}_r)$, and (b) collisional broadening Γ and shift Σ rates that are proportional to the local density: $\Gamma = \rho(R_r)\gamma$ and $\Sigma = \rho(R_r)\sigma$. In this model, we use the measured values $\gamma = 1.47 \times 10^{-20}$ cm^{-1}/cm^{-3}, and $\sigma = 0.75 \times 10^{-20}$ cm^{-1}/cm^{-3} at $T = 475$ K (Allard & Kielkopf 1982). For $T = 2000$ K, we multiply the shift and broadening by a factor 1.4; this factor is obtained from a comparison of line broadening in Na – Ar collision from Jongerius et al. (1981).

Fig. 3 illustrates the absorption spectral line shape of the Na D line embedded in a haze environment of specific Ar density. The two cases considered, with 1000 and 10 000 Ar atoms, include haze seed particles of size given by $a = 40$ a_0. Because of the strong mean-field interaction the line is extremely broad. For comparison, the line profile due to gaseous broadening is represented by the vertical dashed line, since the wavelength width $\Delta\lambda/\lambda_0 \approx n\gamma/\Delta E$ is extremely small at this scale. In a typical planetary atmospheric application $n = 10^{14}$ cm^{-3}, γ is in the range of 10^{-20} cm^{-1}/cm^{-3} (Jongerius et al. 1981; Allard & Kielkopf 1982) and $\Delta E = 16\,964$ cm^{-3} for sodium atom, so that $\Delta\lambda/\lambda_0 \sim 10^{-10}$.

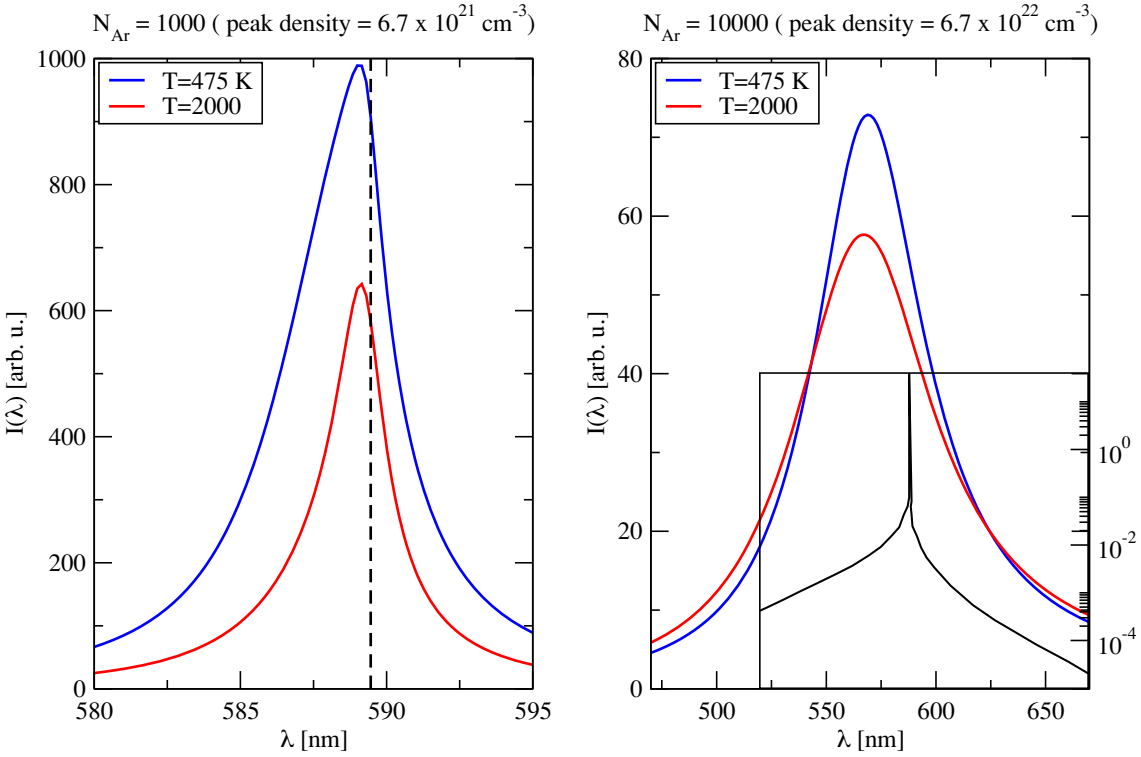

Figure 3. Temperature-dependent spectral line profiles of Na D line embedded in an Ar haze of specific atomic/molecular density. Near the line centre, the temperature dependent is the largest due to collisional effects, and away from the centre, the lines are no longer Lorentzian as the temperature-insensitive mean-field interaction potentials induce asymmetric lineshapes, e.g. Fig. 4. For comparison, we also show in the right figure inset the broadened line due to Na-He collision for which data is available (Burrows & Volobuyev 2003). The pressure broadening affects mainly the line centre and, for the same density, is much narrower than the mean-field broadened lines.

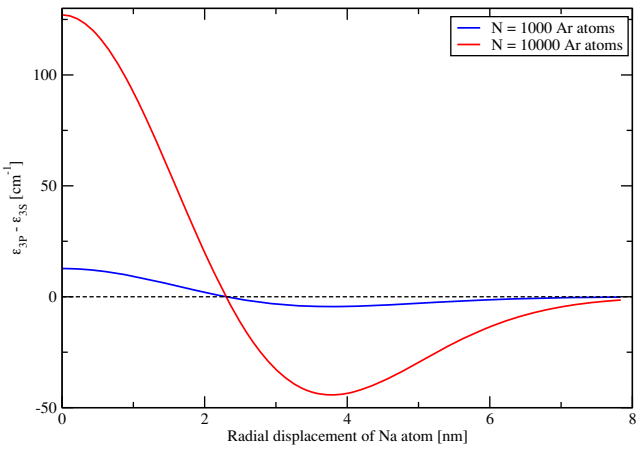

Figure 4. Distortion of the energy difference between levels Na(3S, 3P), due to Ar haze mean field, as a function of the position of the Na atom, for two different numbers of Ar atoms [peak densities $p(R_r = 0)$ at $R_r = 0$]. The haze-sized parameter is $a = 40\ a_0$ (2.12 nm) in both cases, see Section 3.2, corresponding to peak densities of Ar atoms, 6.7×10^{21} and 6.7×10^{22} cm^{-3} for $N = 1000$ and 10 000, respectively.

The probability of finding the sodium atom at some distance R_r is given by the Boltzmann distribution, $p(R_r) = \frac{1}{Z} e^{-\epsilon_{3S}(R_r)/k_B T}$, with normalization $Z = \int_0^\infty e^{-\epsilon_{3S}(R_r)/k_B T}(4\pi R_r^2) dR_r$, $\varepsilon_{3S}(R_r)$ is the mean-field shift in the $3S$ state, see also Fig. 4, and k_B the Boltzmann constant. In the absence of core broadening due to binary collisions, the spectral line profile will contain a characteristic discontinuity at the Na line. The line profiles are asymmetric about the radiator line centre; this expected due to the change in sign of $\Delta\epsilon(R)$, see Fig. 4. *In situ* simulated laboratory measurements of Titan atmospheric aerosol density confirm that effective atomic/molecular densities of aerosol/haze are a few times 10^{22} cm^{-3} for a methane haze (Hörst & Tolbert 2013), in accord with our illustrative haze particle densities.

4 DISCUSSION

Haze influence on absorption/emission spectra strongly depends on mixing ratios of haze particles in atmospheric regions responsible for the formation of transit spectra. The average frequency of the radiator binary collisions with atoms and molecules of ambient gas $\nu_{gas} = n_{gas} v_r \sigma_{gas}$ is usually much larger than the haze-radiator collisional frequency $\nu_{haze} = n_{haze} v_r \sigma_{haze}$, because the number density of haze particles n_{haze} is much smaller than the gas number density n_{gas}. Here, v_r is the radiator velocity and σ_{haze} and σ_{gas} are, respectively, the radiator collisional cross-section with haze and gas particles. Spectral intensities $I_{gas}(\Delta\omega)$ and $I_{haze}(\Delta\omega)$ induced by these two types of collisions are proportional, respectively, to related collisional frequencies ν_{gas} and ν_{haze}, and for $\nu_{gas} \gg \nu_{haze}$, the role of haze-radiator collisions are negligible. Nevertheless, huge shifts of electronic levels in haze/radiator interaction and collisions can provide a dramatic increase of the intensity of spectral wings comparing to the spectra induced in collisions with atmospheric gas. For example, spectra of atomic species, such as Na, K, Fe, Mg, S, and others, can be mostly determined by the radiator interaction with haze nano-particles, if we consider spectral regions of large frequency shift $\Delta\omega = |\omega - \omega_0| \gg \Gamma_{gas} \sim \nu_{gas}$ (Allard &

Kielkopf 1982). Collisions with the gas particles provide mostly small changes of the frequency near the line centre, and the probability $p_{\rm gas}(\Delta\omega)$ to find a large shift $\Delta\omega \gg \Gamma_{\rm gas}$ can be estimated using the spectral Lorentzian width: $p_{\rm gas}(\Delta\omega) \sim \Gamma_{\rm gas}/\Delta\omega \ll 1$. To estimate the spectral intensity ratio $\xi = I_{\rm gas}(\Delta\omega)/I_{\rm haze}(\Delta\omega)$, we make a simplified, and realistic, assumption: a large frequency shift occurs in every haze-radiator collision and the probability of the large frequency shift $\Delta\omega$ in haze collisions $p_{\rm haze}(\Delta\omega) \sim 1$.

The spectral intensity ratio $\xi(\Delta\omega)$ can be evaluated as

$$\xi = \left(\frac{\nu_{\rm gas}\, p_{\rm gas}(\Delta\omega)}{\nu_{\rm haze}\, p_{\rm haze}(\Delta\omega)}\right) = \left(\frac{n_{\rm gas}^2}{n_{\rm haze} n_{\rm atomic}^{\rm haze}}\right)\left(\frac{\sigma_{\rm gas}}{\sigma_{\rm haze}}\right)\left(\frac{m_{\rm e} v_r \sigma_{\rm gas}}{\beta\, 2\pi L\hbar}\right). \quad (7)$$

The averaged value of $\Delta\omega$ in the haze-radiator interaction may be estimated from the mean-field shift in equation (4): $\hbar\Delta\omega \simeq \beta\,(2\pi L\, n_{\rm atomic}^{\rm haze}\, \hbar^2/m_{\rm e})$. The numerical coefficient β shown in the front, scaling the mean-field energy, can vary inside a broad interval $0.1 \leq \beta \leq 1$ depending on the geometrical configuration of haze particles and the symmetry of the radiator electronic states. Examples of numerical calculations of the mean-field energy shifts have been presented in Section 3. The ratio of cross-sections in equation (7) depends on the number of atoms/molecules N in the haze particle and can be estimated as a ratio of the geometrical cross-sections: $\sigma_{\rm gas}/\sigma_{\rm haze} = 1/N^{2/3}$. The haze impact on the atmospheric transit spectra is significant if $\xi(\Delta\omega) \ll 1$.

To illustrate the role of the haze – radiator interaction, we carry out a numerical estimate for ξ for Na radiation in an Earth-like atmosphere. The density of the atmospheric gas near location of the Na-layer could be taken as $n_{\rm gas} \sim 10^{14}$ cm^{-3} with the haze particle density $n_{\rm haze} \sim 10^4$ cm^{-3}. This density of haze particles have been used recently for modelling of the exoplanetary transit spectra (Hörst & Tolbert 2013).[1] For small nano-sized haze particles with $N \sim 10^3$, we estimate the atomic density of these particles as $n_{\rm atomic}^{\rm haze} \sim 10^{22}$ cm^{-3}, with the Na atom velocity taken as $v_{\rm r} \sim 10^3$ cm s^{-1} and the gas collision cross section $\sigma_{\rm gas} \sim 10^{-15}$ cm^2, and $\beta \sim 0.1$. For these conditions, $\xi \sim 0.01 \ll 1$, indicating a strong influence of haze particles on the spectral shape of atomic radiation and flattening of the Na-resonant spectral line.

The haze particles may also form layers, which can be separated from atmospheric metal layers. This separation leads to a significant reduction of the haze particle density $n_{\rm haze}$ in regions occupied by radiators and contributions of haze particles into formation of transit spectra can be negligible ($\xi \gg 1$).

5 SUMMARY

In this work, a unified mean-field framework for the spectral shift and broadening of an atomic radiator in a dense haze environment has been developed. Both collisional interaction, affecting the line centre, and the mean-field energy shifts due the presence of other atomic or molecular perturbers affecting the line wings, in hazy environments, are accounted for. The collisional contribution depends strongly on temperature and has a Lorentzian form, but the mean-field shift is temperature insensitive. The line profiles in hazy environments are asymmetric and significantly broaden because the mean-field generated potential.

The current model has considerable flexibility for extension to different haze environments when chemical composition is mixed, particle densities vary from gaseous to solid phases, and variable porosities. The extension to carbon-bearing molecular haze requires a determination of the electron-molecule scattering length and the electronic wavefunctions for the molecule. Some values of the electron-molecule scattering length are available in the literature, e.g. for e^--CH_4 (methane), the scattering length is about $L = -2.9\ a_0$ (McNaughten, Thompson & Jain 1990), for e^--CO_2 (carbon dioxide), about $L = -7\ a_0$ (Fabrikant 1984), for e^--C_6H_6 (benzene), about $L = -9.21\ a_0$ (Field et al. 2001), and for e^--C_8H_8 (cubane), about $L = -3.5\ a_0$ (Gianturco et al. 2004), but the values depend sensitively on the properties of the molecule and application to specific chemistries will warrant careful analysis and possibly detailed scattering calculations.

The atomic radiator can be embedded within the haze, or outside and can radiate from atomic highly excited states, where strong line shift and broadening may inhibit excitations in the first place. The collisional shift and broadening can be quantitatively calculated at various temperatures with accurate quantum mechanical methods in the impact approximation (Vrinceanu et al. 2004). Our model can be extended to a description of the radiator embedded into liquid or solid matrix. The spectral lines obtained from the analysis above can be input in radiative transfer codes for proper modelling of the properties of the atmospheres and surface, such as the Planetary Atmosphere Generator (Villanueva et al. 2018).

[1]The typical density of Na atoms in the Earth Na layer is around 10^4 cm^{-3}. Ions of different metals Na, K, Fe, Mg, meteorite ashes, and nano-dust particles can be considered as centres of haze nucleation. In quasi-equilibrium conditions, the number density of haze particles should be relatively close to the layer density of metallic atoms and ions.

ACKNOWLEDGEMENTS

ZF was supported by an ITAMP faculty fellowship from an underrepresented institution. HRS, TK, and JFB were supported by an NSF grant to ITAMP. DV was supported by an NSF RISE grant to Texas Southern University.

REFERENCES

Allard N., Kielkopf J., 1982, Rev. Mod. Phys., 54, 1103
Boatz J., Mario E., 1994, J. Chem. Phys., 101, 3472
Boys S. F., Bernardi F., 1970, Mol. Phys., 19, 553
Burrows A., Hubbard W. B., Lunine J. I., Liebert J., 2001, Rev. Mod. Phys., 73, 719
Burrows A., Marley M. S., Sharp C. M., 2000, ApJ, 531, 438
Burrows A., Volobuyev M., 2003, ApJ, 583, 985
Burrows A. S., 2014, Nature, 513, 345
Deming D., Seager S., 2017, JGR-Planets, 122, 53
Demkov Y. N., Ostrovskii V. N., 1988, Zero-Range Potentials and Their Applications in Atomic Physics. Plenum Press, New York, p. 287
Encyclopaedia T. E. P., 2018, The Extrasolar Planets Encyclopaedia. Available at: http://www.exoplanet.eu/
Fabrikant I. I., 1984, J. Phys. B: At. Mol. Opt. Phys., 17, 4223
Fermi E., 1934, Nuovo Cimento, 11, 157
Field D. et al., 2001, J. Phys. B: At. Mol. Opt. Phys., 34, 4371
Fortney J. J., Sudarsky D., Hubeny I., Cooper C. S., Hubbard W. B., Burrows A., Lunine J. I., 2003, ApJ, 589, 615
Fuentealba P., Preuss H., Stoll H., Szentpály L. V., 1982, Chem. Phys. Lett., 89, 418
Gianturco F. A., Lucchese R. R., Grandi A., Sanna N., 2004, J. Chem. Phys., 120, 4172
Greenberg J., Li A., 1999, Space Sci. Rev., 90, 149
Greene C. H., Dickinson A. S., Sadeghpour H. R., 2000, Phys. Rev. Lett., 85, 2458
Hörst S. M. et al., 2018, Nat. Astron., 2, 203

Hörst S. M., Tolbert M. A., 2013, ApJ, 770, L10
Jacquet E., Zanuttini D., Douady J., Giglio E., Gervais B., 2011, J. Chem. Phys., 135, 174503
Jongerius M., Bergen A. V., Hollander T., Alkemade C., 1981, J. Quant. Spectrosc. Radiat. Transfer, 25, 1
Kreidberg L. et al., 2014, Nature, 505, 69
Lendl M., Cubillos P. E., Hagelberg J., Müller A., Juvan I., Fossati L., 2017, A&A, 606, A18
Lenoble J., Mishchenko M. I., Herman H., 2013, in Lenoble J. et al., eds, Aerosol Remote Sensing. Springer-Verlag, Berlin-Heidelberg, p. 13
Marley M. S., Ackerman A. S., Cuzzi J. N., Kitzmann D., 2013, in Mackwell S. J., Simon-Miller A. A., Harder J. W., Bullock M. A., eds, Clouds and Hazes in Exoplanet Atmospheres. Univ. Arizona Press, Tucson, p. 367
McNaughten P., Thompson D. G., Jain A., 1990, J. Phys. B: At. Mol. Opt. Phys., 23, 2405S
Morley C. V., Fortney J. J., Marley M. S., Zahnle K., Line M., Kempton E., Lewis N., Cahoy K., 2015, ApJ, 815, 110
Nicklass A., Dolg M., Stoll H., Preuss H., 1995, J. Chem. Phys., 102, 8942
Ortiz J. L., Moreno F., Molina A., 1996, Icarus, 119, 53
Petrovic Z. L., O'Malley T. F., Crompton R. W., 1995, J. Phys. B: At. Mol. Opt. Phys., 28, 3309
Pont F., Knutson H., Gilliland R. L., Moutou C., Charbonneau D., 2008, MNRAS, 385, 109
Pont F., Sing D. K., Gibson N. P., Aigrain S., Henry G., Husnoo N., 2013, MNRAS, 432, 2917
Rannou P., Hourdin F., McKay C., 2002, Nature, 418, 853
Saxon R. P., Olson R., Liu B., 1977, J. Chem. Phys., 67, 2692
Sciamma-O'Brien E., Upton K., Salama F., 2017, Icarus, 289, 214
Seager S., Deming D., 2010, ARA&A, 48, 631
Seager S., Sasselov D. D., 2000, ApJ, 537, 916
Seignovert B., Rannoua P., Lavvasa P., Cours T., West R. A., 2017, Icarus, 292, 13
Shaffer J.P., Rittenhouse S.T., Sadeghpour H.R., 2018, Nature Communications, 9, 1965
Sing D. K. et al., 2011, A&A, 527, A73
Spake J. J. et al., 2018, Nature, 557, 68
Szasz L., 1985, Pseudo-potential Theory of Atoms and Molecules. Wiley, New York
Szudy J., Baylis W., 1996, Phys. Rep., 266, 127
Tinetti G. et al., 2007, Nature, 448, 169
Tomasko M. G., Karkoschka J., Martinek S., 1986, Icarus, 65, 218
Villanueva G. L., Smith M. D., Protopapa S., Faggi S., Mandell A. M., 2018, J. Quant. Spectrosc. Radiat. Transfer, 217, 86
Vinatier S., Schmitt B., Bézard B., Rannou P., Dauphin C., de Kok R., Jennings D. E., Flasar F. M., 2018, Icarus, 310, 89
Vrinceanu D., Kotochigova S., Sadeghpour H. R., 2004, Phys. Rev. A, 69, 022714
Werner H.-J., et al., 2011, Wiley Interdiscip. Rev.: Comput. Mol. Sci., 2, 242
West R. A., Smith P. H., 1991, Icarus, 90, 330
Wong A., Yung Y. L., Friedson A. J., 2003, Geophys. Res. Lett., 30, 8
Wright J. T. et al., 2011, PASP, 123, 412
Zhang X., Strobel D. F., Imanaka H., 2017, Nature, 551, 352

This paper has been typeset from a TEX/LATEX file prepared by the author.